Bioconjugate Chemistry

pubs.acs.org/bc Article

Chemo-Mechanical Modulation of Cell Motions Using DNA Nanosprings

Deepak Karna, Morgan Stilgenbauer, Sagun Jonchhe, Kazuya Ankai, Ibuki Kawamata, Yunxi Cui, Yao-Rong Zheng, Yuki Suzuki,* and Hanbin Mao*

Cite This: https://dx.doi.org/10.1021/acs.bioconjchem.0c00674 Read Online

ACCESS | Metrics & More | Article Recommendations | Supporting Information

ABSTRACT: Cell motions such as migration and change in cellular morphology are essential activities for multicellular organism in response to environmental stimuli. These activities are a result of coordinated clustering/declustering of integrin molecules at the cell membrane. Here, we prepared DNA origami nanosprings to modulate cell motions by targeting the clustering of integrin molecules. Each nanospring was modified with arginyl-glycyl-aspartic acid (RGD) domains with a spacing such that when the nanospring is coiled, the RGD ligands trigger the clustering of integrin molecules, which changes cell motions. The coiling or uncoiling of the nanospring is controlled, respectively, by the formation or dissolution of an i-motif structure between neighboring piers in the DNA origami nanodevice. At slightly acidic pH (<6.5), the folding of the i-motif leads to the coiling of the nanospring, which inhibits the motion of HeLa cells. At neutrality (pH 7.4), the unfolding of the i-motif allows cells to resume mechanical movement as the nanospring becomes uncoiled. We anticipate that this pH-responsive DNA nanoassembly is valuable to inhibit the migration of metastatic cancer cells in acidic extracellular environment. Such a chemo-mechanical modulation provides a new mechanism for cells to mechanically respond to endogenous chemical cues.

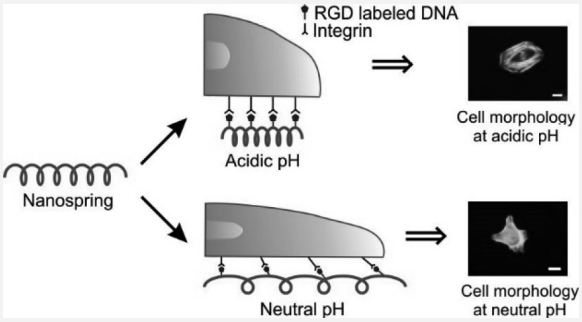

INTRODUCTION

Mechanical motion of cells such as cell migration is a fundamental process involved in the development and maintenance of multicellular tissues. Examples of cell migration include embryonic development, wound healing, vascular growth, and immune responses. The cell migration is accomplished by coordinated movement of cell skeletons, such as actins, that are well orchestrated by cues of chemical or mechanical origin.[1] Many diseases, such as inflammation[2] and tumor formation and metastasis, occur when cell migration goes awry. Targeting cell migration, therefore, becomes a potential means to confine and treat various diseases.

Cell migration is often triggered by the integrin signal pathway.[3] Integrins are transmembrane proteins that are responsible for cell attachment to the extracellular matrix (ECM). At the cell surface, they bind ligands that have peptide domain RGD (arginyl-glycyl-aspartic acid).[4] The binding causes the clustering of the integrin molecules, which activates integrin-mediated processes to modulate cell mechanics,[5] such as migrations and protrusions.[6] This strategy has been used to trigger a mechanical response of the cells by incorporating RGD domains in polymers that are environmentally responsive. Upon the change in temperature[7] or addition of synthetic DNA fragments,[8] the distance between RGD domains varies in these polymers, which changes the clustering state of integrins for the modulation of cell mechanics. Given that the required spatial variation between adjacent RGD groups is on the order of nanometers, it is rather challenging to control the conformation of polymers to the precision that can achieve maximal cell modulations. In addition, the external stimuli such as optothermal input[7] or synthetic DNA fragments[8] present delivery as well as bioavailability issues. To address these problems, it is desirable to use a molecular device whose conformation can be controlled at nanometer precision by native environmental cues. Since tumor cells are exposed to acidic ECM[9−12] while healthy cells have a neutral environment, we seek to use pH as the native chemical cue to modulate cell mechanics via an innovative chemo-mechanical effect.

DNA nanoassembly presents viable materials capable of incorporating pH-sensitive elements for nanometer conformation controls. Invented by Seeman in the 1980s,[13] DNA nanoassembly harnesses the complementarity of DNA strands to assemble into nanostructures. With computer-aided design pioneered by Rothemund,[14] the self-assembly leads to DNA

Received: December 9, 2020
Revised: January 4, 2021

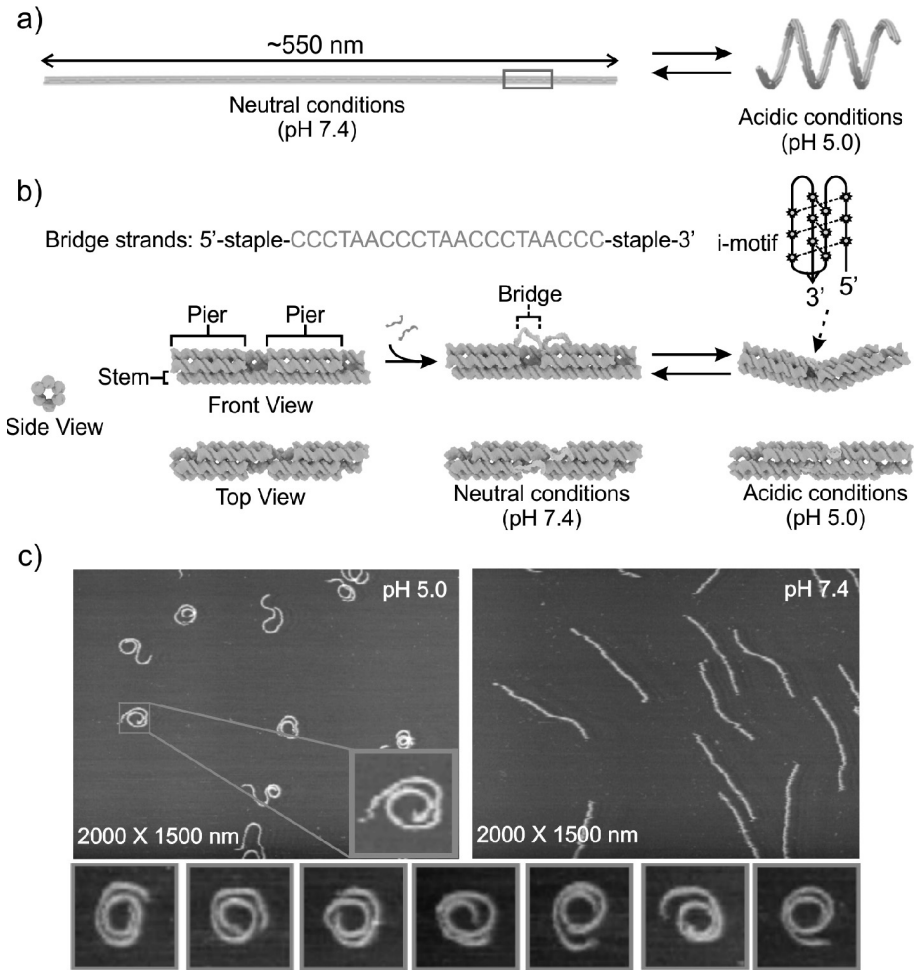

Figure 1. Design of a DNA origami nanospring comprising pH-responsive bendable modules. (a) Reversible transformation of a linear shape into a spring structure through the cumulative actuation of the pH-responsive bendable module. The details of the module structure (red box) are shown in (b). (b) Schematic of the pH-responsive module comprising a stem, two piers, and bridge strands. The bridge strand contained a C-rich DNA repeat sequence in human telomeric region (5′-CCCTAACCCTAACCCTAACCC-3′) flanked with staple sequences that were anchored in each pier. The strand formed an i-motif at acidic conditions (pH 5.0 for example) but became single-stranded at neutrality (pH 7.4), enabling the pH-responsive bending of the module. Transformation of the entire shape was induced by the cumulative effect of each bending, which can be controlled by changing the pH conditions. (c) AFM images of the nanosprings taken at pH 5.0 (left) and pH 7.4 (right). The enlarged images (200 × 200 nm) of different nanosprings formed at pH 5.0 are shown in the inset and the bottom row.

origami structures.[15−20] In a typical procedure, an ssDNA with thousands of nucleotides is used as a template. A number of small DNA fragments are then added to strategically staple together distal regions of the DNA template by the hybridization between the template and the staple strands. This results in desired 2D or 3D DNA nanostructures that are resistant to nuclease activities in cellular conditions.[21] The supramolecular nature of DNA origami self-assembly provides ample space to introduce different functional groups.

In this work, we prepared DNA origami nanosprings. The coils of a nanospring were formed by bringing together adjacent piers in a 6-helix bundle template using i-motif,[22] a pH-responsive DNA secondary structure. At slightly acidic pH, the folding of the i-motif decreases the length of each bridge, facilitating the coiling of the DNA nanospring. At neutral pH, the unfolding of the i-motif allows the separation of the piers, uncoiling the DNA nanospring. After incorporating the integrin ligand, RGD, on the nanospring, more HeLa cells exhibited protruded morphology at neutrality than at slightly acidic environment.[8] In addition, the migration of HeLa cells also showed similar pH dependent behaviors. While cell migration was inhibited at acidic pH in the presence of the RGD-inserted DNA nanospring, the cell motion was not significantly altered at neutrality. Such pH-dependent nanospring behavior is instrumental to inhibit the metastasis of cancer cells in acidic ECM. However, it will not influence the migration of healthy cells, a factor beneficial for physiological processes such as wound healing. This method demonstrates for the first time the mechanical control of cell behaviors using native chemical cues, which represents a new chemo-mechanical approach that can be readily extended to differentially modulate cell actions by exploring many other endogenous chemicals such as metabolic compounds or cell signaling molecules.

■ RESULTS AND DISCUSSION

Formation of Origami Nanosprings is pH-Dependent. Our nanospring (Figure 1a) was folded from a circular ssDNA template (p8064) by the DNA origami method. The DNA origami nanospring contained 37 repeats of a pH-responsive

https://dx.doi.org/10.1021/acs.bioconjchem.0c00674
Bioconjugate Chem. XXXX, XXX, XXX−XXX

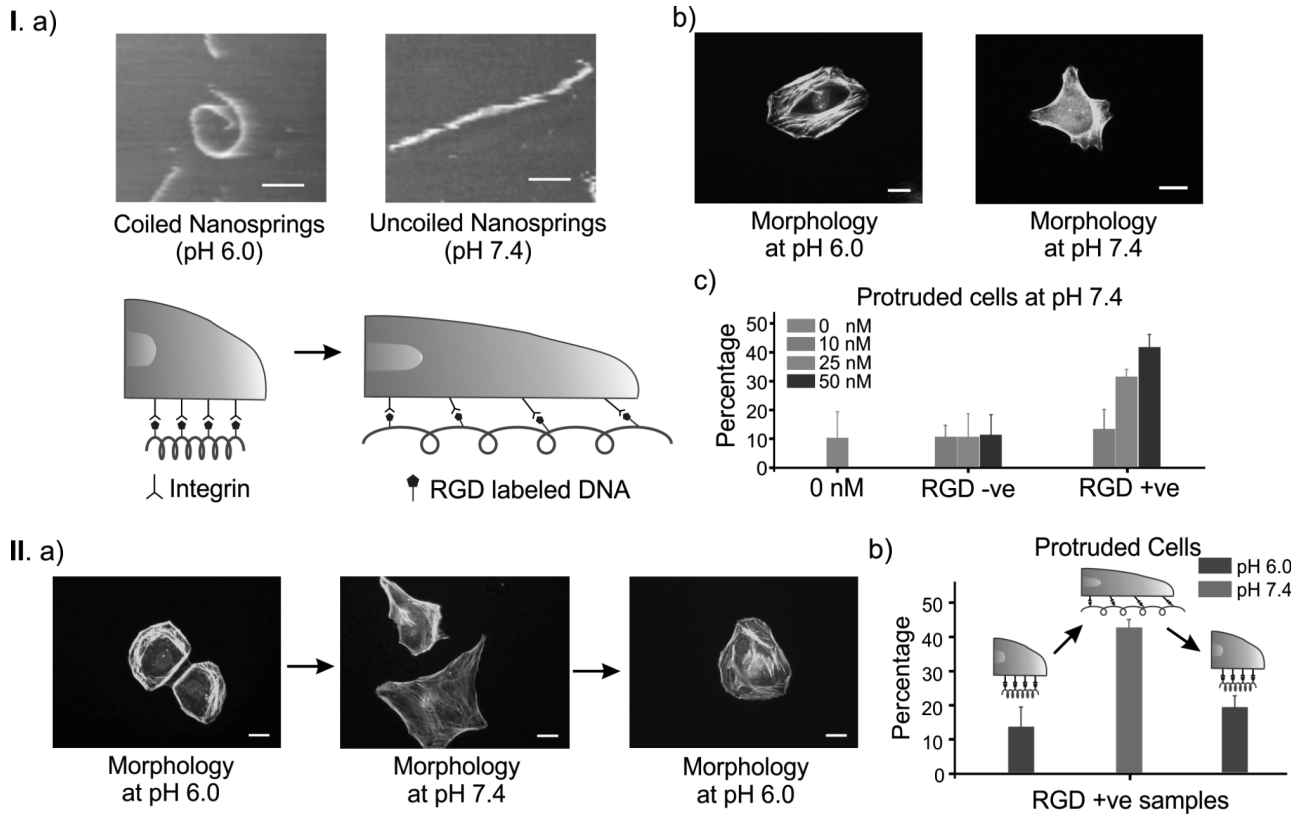

Figure 2. Effect of the RGD embedded nanosprings on the cancer cell morphology. I. (a) Schematic of the change in the HeLa cell morphology due to the RGD embedded nanosprings at pH 6.0 or 7.4. AFM images of origami nanosprings on polylysine coated mica surfaces at respective pH are shown at the top. Scale bars: 100 nm. (b) Representative images of the HeLa cells at different pH. Cells are stained to show nuclei (blue, DAPI) and F-actin (green, FITC-phalloidin). Scale bars: 20 μm. (c) Percentage of protruded HeLa cells at pH 7.4. Error bars represent standard deviations from $N = 32$ cells at each concentration. II. (a) Representative images of the change in the morphology of the HeLa cells in the presence of the RGD labeled nanospring at cycling pH. Cells were stained with the same dyes as described in I. (b). Scale bars: 20 μm. (b) Percentage of protruding population in the HeLa cells at the cycling pH. Error bars represent standard deviations from $N = 32$ cells for each pH sample. See SI for more cell images.

transformable module comprising a stem, two piers, and bridge strands (Figure 1). The bendable stem is a two-helix bundle, while each pier has two additional pairs of two-helix bundles (six helices in total in each module; see Figure 1b). The bridge strand contained a consensus C-rich DNA repeat sequence found in human telomeric region (5′-CCCTAACCCTA-ACCCTAACCC-3′) flanked with staple sequences that were hybridized into each pier. Two bridge strands were incorporated into a single module such that each strand connected to two helices at each of the top layer of the helix bundle. Upon the i-motif formation, the bridge strand contracts, thereby causing the bending of the module (Figure 1b). Via the cumulative effect of this bending throughout the origami nanodevice, the entire shape is transformed from linear into a spring (Figure 1a).

The AFM images (Figure 1c) at acidic pH (5.0) confirmed the spirally coiled structure of nanosprings owing to the cumulative effect of the folding in the i-motifs in the origami bridges. On the other hand, the origami at near-neutral pH (7.4) showed the relaxed linear structure due to the unfolding of the i-motif bridges at neutrality. Additional AFM images of these nanosprings at respective pH are shown in Figure S1. The structures observed at pH 5.0 were consistent with coiled nanosprings (Figure 1c, bottom row). Some spiral and wavy structures observed in AFM images may be due to the collapsing of the nanosprings on the flat mica surface which has been extensively used for AFM imaging. To confirm that the coiling of nanosprings is due to the reversible folding of the i-motifs in the bridges, we replaced the i-motif with polythymine sequences (T_2 or T_{21}). While the first construct (designated as the 2T-NS) showed coiled conformation (Figures S2 and S3), the second origami (designated as the 21T) displayed linear structure (Figure S4). These results demonstrate that the shorter bridge length (such as T_2) between neighboring piers is critical for the formation of nanocoils, which is consistent with the finding of curved origami structures.[23] In addition, neither of the origami nanoconstructs showed pH-dependent structural variations (Figures S2−4), confirming that folded and unfolded i-motifs are the driving forces behind the switchable DNA origami nanospring conformations.

Stability of DNA Nanospring in Serum at Variable pH. DNA origamis have been found to be unstable in extracellular matrix due to presence of nucleases.[24] As most of our further experiments were conducted in cellular environment in the presence of FBS, we first checked the stability of DNA origami under these conditions. The DNA nanosprings were dissolved in DMEM cell growth medium either in the presence or in the absence of FBS at pH 6.0 or 7.4 with incubations for 6 h before they were analyzed by 1.5% agarose gel (see Figure S5a). Lanes 3 and 4 were loaded with nanosprings dissolved in a test tube with duration of 0 h incubated at pH 7.4 in the absence and

https://dx.doi.org/10.1021/acs.bioconjchem.0c00674
Bioconjugate Chem. XXXX, XXX, XXX−XXX

presence of FBS, respectively, while lanes 5 and 6 were those at pH 6.0 in the absence and presence of FBS, respectively. Similarly, lanes 7 to 10 followed the same sequence of loading except that they were incubated for 6 h. With similar gel shifts, no considerable damage to nanosprings was observed within 6 h at pH 7.4. Another set of nanosprings deposited on polylysine coated substrate for 6 h was loaded in lanes 11 to 14. Results indicated that FBS did not have a substantial effect to cause the degradation of DNA nanosprings, especially those on the coated surfaces (28% (surface) vs 36% (solution) of degradation) at pH 6.0 for 6 h. Similarly, the experiment was repeated with 8 h of incubation under similar conditions of pH and substrate (Figure S5b). After 8 h incubation, lanes 10 and 14 indicated some degradation of nanospring (45% and 57% for surface and solution incubations, respectively). These observations implied that the majority of our nanosprings were stable enough to be used for cellular experiments with 6−8 h incubation at pH of 6.0 or 7.4 in the presence of 10% FBS on a polylysine coated surface. Recent discoveries have shown promising improvement on stabilizing DNA origami in the presence of FBS.[25,26] By employing those chemical and photo-cross-linking strategies, the stability of our DNA origami can hence be further increased.

The i-Motif Nanosprings Modulate Cell Mechanics. It has been known that the anchorage of the RGD in the ECM to the integrin receptors causes clustering of integrin molecules at the cell surface, which, in turn, modulates cell mechanics.[27] To achieve the pH-dependent effect of DNA nanosprings on the cell motions, therefore, we incorporated RGD domains into the DNA nanosprings. To this end, the pH-responsive nanosprings were modified with RGD labeled DNA with a spacing of 252 nts (∼86 nm) in the origami backbone using extended DNA staples (see SI for details). To confirm that all the RGD sites were occupied by specific staple strands, we performed an experiment substituting the RGD sites in staples with biotin modified strands and consequently conjugated with streptavidin molecules. AFM images (Figure S6) showed seven such expected sites on the nanosprings that could hold specific molecules. In addition, the spacing of neighboring modifications was 82 ± 8 nm (N = 36), which was consistent with the theoretical spacing (252 bp = 85.7 nm). Such spacing was chosen based on the fact that the activation of integrin clustering required a distance of approximately 70 nm[28] between integrin molecules. The shift of the DNA band in agarose gel confirmed proper ligation of RGD to nanosprings (Figure S7). AFM images (Figure S8) confirmed that the integration of RGD domains onto the nanospring does not alter the conformational switch of nanospring with respect to pH change. Given different pH environment of the ECM for tumor cells (acidic) and normal cells (close to neutral),[9−12] we expected a change in the coiling of nanosprings in these two environments. Such a switch between coiled (acidic) and uncoiled (neutral) nanosprings causes a significant change in the distance between consecutive RGD labels, which results in the clustering of integrins at acidic condition only. The clustering of integrins then triggers biochemical pathways of the HeLa cells,[3] leading to protruding cellular morphology at neutrality but a normal cell shape at acidic ECM (Figure 2 I.a).

To evaluate this switching effect, we incubated overnight 10−50 nM of RGD-embedded nanosprings (designated as RGD + ve) and nanosprings without RGD (designated as RGD − ve) in a 5 mM MES buffer (15 mM $MgCl_2$ + 1 mM EDTA, pH 5.5) on dishes coated with poly(D-lysine), whose positive charges facilitated the attachment of negatively charged DNA origami on the surface. Next, the dishes were washed thoroughly with an MES buffer (pH 6.0), and then medium containing 10% FBS was introduced to incubate HeLa cells. This pH (pH 6.0) was used to mimic slightly acidic ECM environment of tumor cells.[9−12] AFM images still showed the coiling of the nanosprings modified with RGD at this slightly acidic pH (Figure 2 I.a). After 6−8 h of incubation at 37 °C provided with 5% CO_2, HeLa cells with protrusions were counted. Analysis of protruding morphology was described by Li's group.[8] After counting, the buffer was changed to pH 7.4 for overnight incubation, followed by another counting of protruding cells. Figure 2 I.b shows the morphology of HeLa cells at respective pH. The results (Figure 2 I.c) indicated that the percentage of the HeLa cells having protruded morphology increased in a concentration dependent manner for the nanosprings with RGD (RGD + ve) compared to that of the nanosprings without RGD (RGD − ve). Such results can be attributed to the fact that RGD + ve nanosprings bound strongly to the integrin receptors on HeLa cells via RGD−integrin interactions.[29] Without RGD embedded in the nanosprings (RGD − ve), the percentage of protruding cells remained similar irrespective of different concentrations of the origami nanosprings at neutral pH.

In a control experiment to understand the reversible conformation change of nanosprings on the polylysine coated surface, we coated the mica surface with polylysine and observed the AFM images at pH 6.0 and 7.4 (Figure S9). Reversible conformational changes were examined for two cycles on the polylysine-treated mica surface. The results showed that nanosprings retained surface mobility and underwent pH-dependent coiling/uncoiling on the polylysine-coated surface.

Next, we investigated the reversible effect of the RGD + ve nanosprings on the HeLa cells by cycling the pH from slightly acidic (pH 6.0) to neutral (pH 7.4) and back to acidic (pH 6.0) conditions. After counting the number of protruding HeLa cells at pH 7.4, which showed significant increase in Figure 2 II.b, the pH was reverted back to pH 6.0 and it was incubated for 4 h. Protruding cells were again counted, which showed a markedly decreased percentage compared to pH 7.4 (Figure 2 II.b). These experiments indicated pH-dependent reversible modulations on cell morphologies, which are fully consistent with the coiling and uncoiling of the DNA origami nanosprings at different pH. Such an observation implies that the nanosprings can serve as a probe to measure the lateral force for clustering/declustering of integrin molecules to control the protrusions on the cell surface. Since the average force to disrupt the i-motif is ∼25 pN (Figure S10), it is evident that the 25 pN is sufficient for clustering/declustering of integrins. In addition, from Figure S9 where the pH change stimulates coiling/uncoiling of DNA origami irrespective of polylysines on the surface, it can also be ascertained that the lateral force required to cause the coiling and uncoiling of nanospring is larger than the interaction force between surface immobilized polylysine and nanosprings.

Finally, we performed scratch assay to evaluate the cell migration rates when monolayer HeLa cells with 100% confluency were exposed to either the RGD + ve or RGD − ve nanospring coated surface. Following the protocol established by the Guan group,[30] we quantified the migration rates at the edge of scratches after 8 h of cell incubation for 3 independent samples. Monolayer HeLa cells that were cultured

https://dx.doi.org/10.1021/acs.bioconjchem.0c00674
Bioconjugate Chem. XXXX, XXX, XXX−XXX

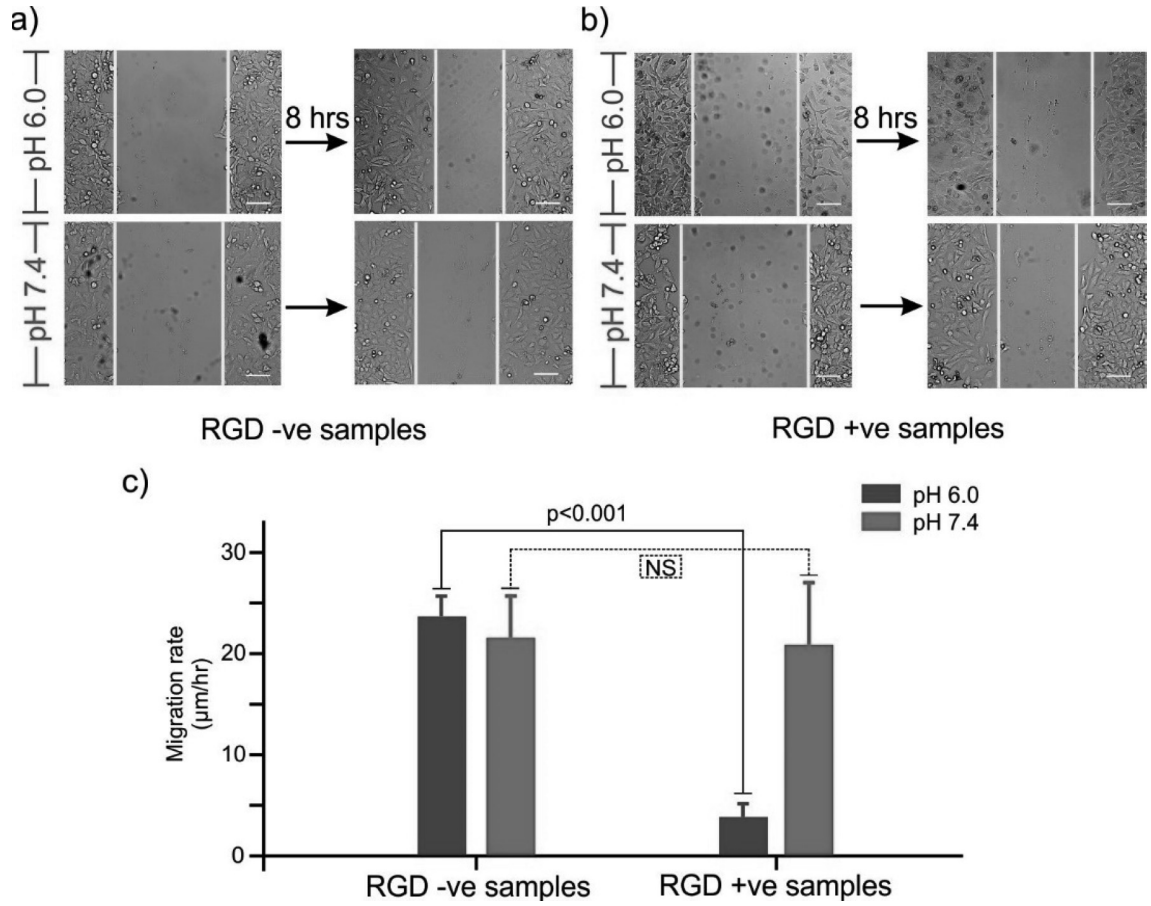

Figure 3. Effect of RGD embedded nanosprings on cell migrations. Representative images of the HeLa cells showing migrations after 8 h at pH 6.0 and 7.4 for the RGD − ve samples (a) and RGD + ve nanospring samples (b). Scale bar: 100 μm. (c) Statistical analyses of the migration rates of the HeLa cells. Error bars indicate standard deviations from 3 independent experiments for each sample. Migration rate in the presence of the RGD-labeled nanosprings is slower than that without RGD at pH 6 ($p < 0.001$, one-tailed-t test). Migration rates are similar at pH 7.4. NS depicts no significant difference.

on a dish coated with the RGD + ve nanosprings showed lower migration rates ($p < 0.001$) compared to that coated with the RGD − ve nanosprings at pH 6.0 (Figure 3). The lower migration rates may represent the cellular processes originated by the clustered integrins[31] bound to the RGD in coiled origami nanosprings under slightly acidic condition. As a control, no significant difference in migration rates was observed between RGD + ve and − ve nanosprings at neutral pH. In both samples, the HeLa cells were protruded, indicating extended nanosprings at neutrality as shown in Figure 3. From these experiments, we confirm that our nanosprings can inhibit the migration of the HeLa cells in acidic ECM in which tumor cells are often exposed. These nanosprings are not expected to significantly affect the migration of cells grown in regular neutral environment. When live/dead cell assays[32] were performed, we found more than 92% HeLa cells were alive when incubated with various nanospring samples for 8 h in either pH 6.0 or 7.4 (Figure S11). This indicated that the DNA origami nanosprings presented nonsignificant toxicity to cells.

■ CONCLUSION

In summary, we successfully synthesized DNA origami nanosprings that change their mechanical structures in the narrow pH range of 6.0−7.4. These DNA nanosprings were exploited to modulate cell morphologies and migrations by targeting the integrins on cell membranes. Since these pH sensitive origami nanoassemblies allowed a unique advantage to inhibit the movement of HeLa cells in acidic ECM, we expect our origami nanodevices to be particularly beneficial to target tumorigenic metastases. The unique mechanical modulation of cell behaviors in response to innate chemical cues provides a new and generic chemo-mechanical approach to precisely control cell functions.

■ EXPERIMENTAL SECTION

Preparation of DNA Origami Nanosprings. DNA origami structures were designed using caDNAno software[33] for strand routing and CanDo[34,35] for the prediction. Designed assembly was prepared by mixing scaffold DNA (p8064) with staple strands and bridge strands in folding buffer (5 mM Tris-HCl, 1 mM EDTA, and 15 mM $MgCl_2$) maintained at 65 °C for 15 min, which was then annealed by reducing temperature to 45 °C at a rate of −1.0 °C/h. Next, the annealed mixture was purified and mixed with precipitation buffer (15% PEG 8000, 5 mM Tris-HCl, 1 mM EDTA, and 505 mM NaCl). Finally, the solution was centrifuged, and pellet was dissolved in buffer of required pH for further analysis (see SI for details).

Atomic Force Microscopy Observation. AFM imaging was performed using a tip scan high-speed AFM (BIXAM, Olympus, Tokyo, Japan) that was improved based on a

https://dx.doi.org/10.1021/acs.bioconjchem.0c00674
Bioconjugate Chem. XXXX, XXX, XXX−XXX

previously developed prototype AFM.[36] A drop (2 μL) of the sample (~1 nM) in the buffer of designated pH (pH 7.4:5 mM Tris-HCl (pH 7.4), 15 mM $MgCl_2$, and 1 mM EDTA; pH 5.0:5 mM MES-KOH (pH 5.0), 15 mM $MgCl_2$, 1 mM EDTA) was deposited onto a freshly cleaved mica surface or 0.05% APTES (3-aminopropyl triethoxysilane)-treated mica surface and incubated for 1 min. The surface was subsequently rinsed with 10 μL of the same buffer. Small cantilevers (9 μm long, 2 μm wide, and 100 nm thick; USC-F0.8-k0.1-T12, Nanoworld) having a spring constant of ~0.1 N/m and a resonant frequency of ~300−600 kHz in water were used to scan the sample surface. The 320 × 240-pixel images were collected at a scan rate of 0.5 frames per second (fps). The images were flattened using an AFM scanning software (Olympus) and ImageJ (http://imagej.nih.gov/ij/) software.

Assessment of the RGD Embedded Nanosprings on Cancer Cell Morphology. Previously maintained HeLa cell lines (see SI for details) were used for study of cellular assays. The imaging dishes (35 mm diameter dish, 10 mm diameter microwell, poly(D-lysine) coated, MatTek Corporation) were coated with RGD + ve and RGD − ve nanospring samples overnight. A total of ~500 HeLa cells were seeded onto the dish with complete media at pH 6.0, and were allowed to adhere for 6−8 h. Upon attachment to the dish, morphology of HeLa cells was recorded on the Olympus IX70 microscope with a 40× objective. To examine the reversibility of morphology change, the media at pH = 7.4 were replaced to the media at pH = 6.0 and incubated for an additional 4 h. The cell images were processed using ImageJ. For actin staining, the media were removed, and cells were washed once with PBS. The cells were then fixed and permeabilized using BD Cytofix/Cytoperm kit (Thermo Fisher Scientific). 100 μL of BD Fixation and Permeabilization Solution was added to the cells and incubated in the dark at 4 °C for 20 min. The solution was removed, and then cells were washed twice with 250 μL of 1× BD Perm/Wash Buffer. The solution was removed and 200 μL of 1× Perm/Wash Buffer containing phalloidin-FITC and Hoechst dyes was added. The cells were incubated at room temperature for 30 min. After incubation, the cells were washed twice with PBS and images were acquired on the microscope. The images were processed using ImageJ.

Scratch Assays. A total of ~50,000 HeLa cells were seeded overnight on poly(D-lysine) coated imaging dishes (MatTek Corporation) that had been incubated with DNA origamis at either pH 6.0 or 7.4. Next, the monolayer was scratched using a P10 pipet tip. The dishes were then washed once with PBS, and the media was replaced at pH 6.0 or 7.4. Migration was monitored after 8 h on the Olympus IX70 microscope with a 10× objective, and the images were acquired. The images were processed using ImageJ.

■ ASSOCIATED CONTENT

Supporting Information

The Supporting Information is available free of charge at https://pubs.acs.org/doi/10.1021/acs.bioconjchem.0c00674.

Experimental details, Preparation of DNA origami nanosprings, Preparation of RGD-conjugated oligodeoxynucleotides, Preparation of RGD-conjugated DNA origami nanosprings, Cell lines and cell culture, Agarose gel electrophoresis of RGD-conjugated nanosprings, Stability assay of nanosprings in different conditions, Sites specific for RGD conjugation, Additional AFM images of i-motif nanospring, 2T nanospring, and 21T nanospring, AFM images of nanosprings on polylysine coated mica surface, Additional stained cancer cell images, F-X curve and unfolding force histogram for the telomere i-motif, Live/Dead assay, and Origami nanospring design (PDF)

■ AUTHOR INFORMATION

Corresponding Authors

Yuki Suzuki − *Frontier Research Institute for Interdisciplinary Sciences and Department of Robotics, Graduate School of Engineering, Tohoku University, Aoba-ku, Sendai 980-8578, Japan*; orcid.org/0000-0003-1848-0105; Email: ysuzuki79r@molbot.mech.tohoku.ac.jp

Hanbin Mao − *Department of Chemistry & Biochemistry, Kent State University, Kent, Ohio 44242, United States*; orcid.org/0000-0002-6720-9429; Email: hmao@kent.edu

Authors

Deepak Karna − *Department of Chemistry & Biochemistry, Kent State University, Kent, Ohio 44242, United States*; orcid.org/0000-0003-3370-0997

Morgan Stilgenbauer − *Department of Chemistry & Biochemistry, Kent State University, Kent, Ohio 44242, United States*

Sagun Jonchhe − *Department of Chemistry & Biochemistry, Kent State University, Kent, Ohio 44242, United States*; orcid.org/0000-0003-4361-6641

Kazuya Ankai − *Frontier Research Institute for Interdisciplinary Sciences, Tohoku University, Aoba-ku, Sendai 980-8578, Japan*

Ibuki Kawamata − *Department of Robotics, Graduate School of Engineering, Tohoku University, Aoba-ku, Sendai 980-8579, Japan; Natural Science Division, Faculty of Core Research, Ochanomizu University, Bunkyo-ku, Tokyo 112-8610, Japan*; orcid.org/0000-0002-1955-8827

Yunxi Cui − *Department of Chemistry & Biochemistry, Kent State University, Kent, Ohio 44242, United States; College of Life Sciences, Nankai University, Tianjin 300071, China*; orcid.org/0000-0002-3830-3336

Yao-Rong Zheng − *Department of Chemistry & Biochemistry, Kent State University, Kent, Ohio 44242, United States*; orcid.org/0000-0003-4605-1121

Complete contact information is available at: https://pubs.acs.org/10.1021/acs.bioconjchem.0c00674

Notes

The authors declare no competing financial interest.

■ ACKNOWLEDGMENTS

H.M. thanks NIH (R01 CA236350) and NSF (CBET-1904921, for mechanical chracterizations of DNA structures) for support. Y.S. thanks Japan Society for the Promotion of Science (JSPS) Grant-in-Aid for Scientific Research (KAKENHI; grant numbers 18K19831, 18KK0139, and 19H04201). Y.Z. thanks the financial support provided by the startup fund, Farris Family Innovation Fellowship, and LaunchPad Award provided by Kent State University.

REFERENCES

(1) Mak, M., Spill, F., Kamm, R. D., and Zaman, M. H. (2016) Single-Cell Migration in Complex Microenvironments: Mechanics and Signaling Dynamics. *J. Biomech. Eng. 138* (2), 1 DOI: 10.1115/1.4032188.

(2) Arakelyan, A., Nersisyan, L., Poghosyan, D., Khondkaryan, L., Hakobyan, A., Löffler-Wirth, H., Melanitou, E., and Binder, H. (2017) Autoimmunity and autoinflammation: A systems view on signaling pathway dysregulation profiles. *PLoS One 12* (11), e0187572.

(3) Clark, E. A., and Brugge, J. S. (1995) Integrins and signal transduction pathways: the road taken. *Science 268* (5208), 233.

(4) Pierschbacher, M. D., and Ruoslahti, E. (1984) Cell attachment activity of fibronectin can be duplicated by small synthetic fragments of the molecule. *Nature 309* (5963), 30−33.

(5) Miyamoto, S., Akiyama, S. K., and Yamada, K. M. (1995) Synergistic roles for receptor occupancy and aggregation in integrin transmembrane function. *Science 267* (5199), 883.

(6) DeMali, K. A., and Burridge, K. (2003) Coupling membrane protrusion and cell adhesion. *J. Cell Sci. 116* (12), 2389−2397.

(7) Liu, Z., Liu, Y., Chang, Y., Seyf, H. R., Henry, A., Mattheyses, A. L., Yehl, K., Zhang, Y., Huang, Z., and Salaita, K. (2016) Nanoscale optomechanical actuators for controlling mechanotransduction in living cells. *Nat. Methods 13* (2), 143−146.

(8) Zhang, K., Deng, R., Sun, Y., Zhang, L., and Li, J. (2017) Reversible control of cell membrane receptor function using DNA nano-spring multivalent ligands. *Chemical Science 8* (10), 7098−7105.

(9) Tannock, I. F., and Rotin, D. (1989) Acid pH in Tumors and Its Potential for Therapeutic Exploitation. *Cancer Res. 49* (16), 4373−4384.

(10) Hao, G., Xu, Z. P., and Li, L. (2018) Manipulating extracellular tumour pH: an effective target for cancer therapy. *RSC Adv. 8* (39), 22182−22192.

(11) Griffiths, J. R. (1991) Are cancer cells acidic? *Br. J. Cancer 64*, 425−427.

(12) Anderson, M., Moshnikova, A., Engelman, D. M., Reshetnyak, Y. K., and Andreev, O. A. (2016) Probe for the measurement of cell surface pH in vivo and ex vivo. *Proc. Natl. Acad. Sci. U. S. A. 113* (29), 8177−8181.

(13) Seeman, N. C. (1982) Nucleic acid junctions and lattices. *J. Theor. Biol. 99* (2), 237−247.

(14) Rothemund, P. W. K. (2006) Folding DNA to Create Nanoscale Shapes and Patterns. *Nature 440*, 297−302.

(15) Hong, F., Zhang, F., Liu, Y., and Yan, H. (2017) DNA Origami: Scaffolds for Creating Higher Order Structures. *Chem. Rev. 117* (20), 12584−12640.

(16) Douglas, S. M., Dietz, H., Liedl, T., Högberg, B., Graf, F., and Shih, W. M. (2009) Self-assembly of DNA into nanoscale three-dimensional shapes. *Nature 459* (7245), 414−418.

(17) Douglas, S. M., Bachelet, I., and Church, G. M. (2012) A Logic-gated Nanorobot for Targeted Transport of Molecular Payloads. *Science 335*, 831−4.

(18) Ke, Y., Castro, C., and Choi, J. H. (2018) Structural DNA Nanotechnology: Artificial Nanostructures for Biomedical Research. *Annu. Rev. Biomed. Eng. 20* (1), 375−401.

(19) Dietz, H., Douglas, S. M., and Shih, W. M. (2009) Folding DNA into twisted and curved nanoscale shapes. *Science (Washington, DC, U. S.) 325* (5941), 725−730.

(20) Han, D., Pal, S., Nangreave, J., Deng, Z., Liu, Y., and Yan, H. (2011) DNA Origami with Complex Curvatures in Three-Dimensional Space. *Science 332*, 342−346.

(21) Mei, Q., Wei, X., Su, F., Liu, Y., Youngbull, C., Johnson, R., Lindsay, S., Yan, H., and Meldrum, D. (2011) Stability of DNA origami nanoarrays in cell lysate. *Nano Lett. 11* (4), 1477−1482.

(22) Gehring, K., Leroy, J. L., and Guéron, M. (1993) A tetrameric DNA structure with protonated cytosine•cytosine base pairs. *Nature 363*, 561−564.

(23) Suzuki, Y., Kawamata, I., Mizuno, K., and Murata, S. (2020) Large Deformation of a DNA-Origami Nanoarm Induced by the Cumulative Actuation of Tension-Adjustable Modules. *Angew. Chem., Int. Ed. 59* (15), 6230−6234.

(24) Hahn, J., Wickham, S. F. J., Shih, W. M., and Perrault, S. D. (2014) Addressing the instability of DNA nanostructures in tissue culture. *ACS Nano 8* (9), 8765−8775.

(25) Anastassacos, F. M., Zhao, Z., Zeng, Y., and Shih, W. M. (2020) Glutaraldehyde Cross-Linking of Oligolysines Coating DNA Origami Greatly Reduces Susceptibility to Nuclease Degradation. *J. Am. Chem. Soc. 142* (7), 3311−3315.

(26) Gerling, T., Kube, M., Kick, B., and Dietz, H. (2018) Sequence-programmable covalent bonding of designed DNA assemblies. *Sci. Adv. 4* (8), eaau1157.

(27) Changede, R., and Sheetz, M. (2017) Integrin and cadherin clusters: A robust way to organize adhesions for cell mechanics. *BioEssays 39* (1), e201600123.

(28) Dalby, M. J., Gadegaard, N., and Oreffo, R. O. C. (2014) Harnessing nanotopography and integrin−matrix interactions to influence stem cell fate. *Nat. Mater. 13*, 558.

(29) Orgovan, N., Peter, B., Bősze, S., Ramsden, J. J., Szabó, B., and Horvath, R. (2015) Dependence of cancer cell adhesion kinetics on integrin ligand surface density measured by a high-throughput label-free resonant waveguide grating biosensor. *Sci. Rep. 4* (1), 4034.

(30) Liang, C.-C., Park, A. Y., and Guan, J.-L. (2007) In vitro scratch assay: a convenient and inexpensive method for analysis of cell migration in vitro. *Nat. Protoc. 2* (2), 329−333.

(31) Huttenlocher, A., and Horwitz, A. R. (2011) Integrins in cell migration. *Cold Spring Harbor Perspect. Biol. 3* (9), a005074−a005074.

(32) Panseri, S., Cunha, C., D'Alessandro, T., Sandri, M., Giavaresi, G., Marcacci, M., Hung, C. T., and Tampieri, A. (2012) Intrinsically superparamagnetic Fe-hydroxyapatite nanoparticles positively influence osteoblast-like cell behaviour. *J. Nanobiotechnol. 10* (1), 32.

(33) Douglas, S. M., Marblestone, A. H., Teerapittayanon, S., Vazquez, A., Church, G. M., and Shih, W. M. (2009) Rapid prototyping of 3D DNA-origami shapes with caDNAno. *Nucleic Acids Res. 37* (15), 5001−5006.

(34) Castro, C. E., Kilchherr, F., Kim, D. N., Shiao, E. L., Wauer, T., Wortmann, P., Bathe, M., and Dietz, H. (2011) A primer to scaffolded DNA origami. *Nat. Methods 8* (3), 221−9.

(35) Kim, D. N., Kilchherr, F., Dietz, H., and Bathe, M. (2012) Quantitative prediction of 3D solution shape and flexibility of nucleic acid nanostructures. *Nucleic Acids Res. 40* (7), 2862−8.

(36) Suzuki, Y., Sakai, N., Yoshida, A., Uekusa, Y., Yagi, A., Imaoka, Y., Ito, S., Karaki, K., and Takeyasu, K. (2013) High-speed atomic force microscopy combined with inverted optical microscopy for studying cellular events. *Sci. Rep. 3*, 2131.

https://dx.doi.org/10.1021/acs.bioconjchem.0c00674
Bioconjugate Chem. XXXX, XXX, XXX−XXX